Journal of Biomechanics 116 (2021) 110209

Contents lists available at ScienceDirect

Journal of Biomechanics

journal homepage: www.elsevier.com/locate/jbiomech
www.JBiomech.com

Impact of prosthetic mitral valve orientation on the ventricular flow field: Comparison using patient-specific computational fluid dynamics

Jonas Lantz [a,b], Sophia Bäck [a,b], Carl-Johan Carlhäll [b,c], Ann Bolger [c,d], Anders Persson [b,e], Matts Karlsson [b,f], Tino Ebbers [a,b,*]

[a] Division of Cardiovascular Medicine, Department of Health, Medicine and Caring Sciences, Linköping University, Linköping, Sweden
[b] Center for Medical Image Science and Visualization (CMIV), Linköping University, Linköping, Sweden
[c] Department of Clinical Physiology in Linköping, and Department of Health, Medicine and Caring Sciences, Linköping University, Linköping, Sweden
[d] Department of Medicine, University of California, San Francisco, United States
[e] Division of Radiology, Department of Health, Medicine and Caring Sciences, Linköping University, Linköping, Sweden
[f] Division of Applied Thermodynamics and Fluid Mechanics, Department of Management and Engineering, Linköping University, Sweden

ARTICLE INFO

Article history:
Accepted 14 December 2020

Keywords:
Computational fluid dynamics
Virtual implantation
Mitral valve
Computed tomography
4D flow CT

ABSTRACT

Significant mitral valve regurgitation creates progressive adverse remodeling of the left ventricle (LV). Replacement of the failing valve with a prosthesis generally improves patient outcomes but leaves the patient with non-physiological intracardiac flow patterns that might contribute to their future risk of thrombus formation and embolism.

It has been suggested that the angular orientation of the implanted valve might modify the postoperative distortion of the intraventricular flow field. In this study, we investigated the effect of prosthetic valve orientation on LV flow patterns by using heart geometry from a patient with LV dysfunction and a competent native mitral valve to calculate intracardiac flow fields with computational fluid dynamics (CFD). Results were validated using *in vivo* 4D Flow MRI. The computed flow fields were compared to calculations following virtual implantation of a mechanical heart valve oriented in four different angles to assess the effect of leaflet position. Flow patterns were visualized in long- and short-axes and quantified with flow component analysis. In comparison to a native valve, valve implantation increased the proportion of the mitral inflow remaining in the basal region and further increased the residual volume in the apical area. Only slight changes due to valve orientation were observed.

Using our numerical framework, we demonstrated quantitative changes in left ventricular blood flow due to prosthetic mitral replacement. This framework may be used to improve design of prosthetic heart valves and implantation procedures to minimize the potential for apical flow stasis, and potentially assist personalized treatment planning.

1. Introduction

It is widely accepted that mitral valve prostheses, particularly mechanical valves, strongly affect left ventricular (LV) hemodynamics (Faludi et al., 2010; Garitey et al., 1995; Meschini et al., 2018; Nguyen et al., 2018; Pierrakos et al., 2004; Querzoli et al., 2010; Sotiropoulos et al., 2016; Yoganathan et al., 2004). The type, size and orientation of the prosthesis, in combination with the individual-specific ventricular geometry and function, create complex and patient-specific flow patterns. While patient outcome and quality of life generally improve after implantation of a prosthetic mechanical valve, long-term risks remain. The most serious complication related to mechanical heart valves is the formation of thrombus and thromboembolism (Chandran, 2010; Laplace et al., 2004; Sotiropoulos et al., 2016; Yoganathan et al., 2004), which requires long-term anticoagulant therapy. Abnormal flow across the mechanical valve are believed to be the major factor resulting in thrombus deposition, as high flow shear stresses can initiate platelet activation and subsequent embolic complications (Chandran, 2010). The risk of embolism has been reported to be higher for mechanical valves in the mitral position compared to other prosthetic types and valve locations (Cannegieter et al., 1994; Chandran, 2010). There have been reports that thrombus risk can been linked to the specific implantation approach selected at

* Corresponding author at: Department of Health, Medicine and Caring Sciences, Linköping University, SE-58183 Linköping, Sweden.
E-mail address: Tino.Ebbers@liu.se (T. Ebbers).

https://doi.org/10.1016/j.jbiomech.2020.110209
0021-9290/

surgery (Pibarot and Dumesnil, 2009; Sotiropoulos et al., 2016), and that the directional orientation of the prosthesis in the atrioventricular annulus can have a significant effect on intraventricular flow fields (Choi et al., 2014; Mächler et al., 2007, 2004; Pierrakos and Vlachos, 2006; Saaid et al., 2018; Stijnen et al., 2001; Van Rijk-Zwikker et al., 1996; Westerdale et al., 2015). Some have proposed that bileaflet valves should be implanted in an anti-anatomic position (perpendicular to the major axis of the native leaflets) to recreate more physiological postoperative flow patterns and to ensure more unobstructed leaflet motion (Laub et al., 1992; Pibarot and Dumesnil, 2009; Van Rijk-Zwikker et al., 1996).

Understanding the postoperative flow conditions could provide important insights into the patient's long-term clinical outcome (Nguyen et al., 2018). In vivo measurements, like 4D flow MRI (Dyverfeldt et al., 2015), can only describe the post implantation flow field specific to that individual's prosthetic valve orientation. Predictive numerical models could provide *a priori* information that might potentially complement or surpass traditional assessment methods.

Cardiac flow patterns are complex and time-varying, rich with vortical structures of different sizes and dynamics, and as such require high-resolution computational techniques for their accurate assessment (Sotiropoulos et al., 2016). Computational studies of ventricular flow are becoming more and more frequent, but as noted by Chandran (Chandran, 2010), detailed and realistic computational analyses for prosthetic heart valves require both realistic 3D geometries and appropriate physiological boundary conditions that match those to which the valve is subjected during the cardiac cycle. Such analyses must be validated by comparison to *in vivo* data.

Several studies have simulated mechanical heart valves in the aortic position (Bianchi et al., 2019; Singh-Gryzbon et al., 2020; Wu et al., 2016). From a technical point of view, the mechanical aortic valve is easier to simulate than the mitral valve for several reasons: i) the aortic transvalvular flow rate can be prescribed directly if the flow rate is known in the aorta, for example from MRI flow measurements, ii) the motion of the aorta and aortic sinuses are generally assumed to have negligible effect on the flow patterns, and iii) the aorta is often assumed to be a rigid pipe-like structure, which greatly simplifies the analysis. In contrast, the analysis of the mitral valve is significantly more complicated (Walczak et al., 2019). The mitral transvalvular flow rate is determined by the ventricular volume change which must be accurately measured. The translation and shape change of the LV endocardial surface, the thickening of the papillary muscles and the folding/unfolding of the mural trabeculations during contraction and relaxation all contribute to the volume change, significantly complicating the analysis. We have recently developed a numerical framework (Lantz et al., 2018, 2016) to compute intracardiac blood flow based on high resolution clinical CT images which can depict these features. Correlation with *in vivo* flow measurements has been very good (Lantz et al., 2018).

The aim of this study was to investigate how LV flow patterns are affected by deployment of a mechanical valve in the mitral position. In vivo flow measurements from 4D Flow MRI and numerical simulations based on CT images of a patient with an enlarged and hypocontractile LV and a competent native valve were compared to validate the simulation. Simulations representing postoperative flow fields after implantation of a mechanical bileaflet valve in four different orientations were then assessed.

2. Materials and methods

The imaging methods and computational model used in this study for the native valve are briefly described here. More details can be found in the supplementary material and in previous publications (Lantz et al., 2018, 2016).

2.1. CT and MR imaging

A patient with known cardiovascular disease and clinical referral for coronary CT angiography underwent a 4D flow MRI acquisition within two hours after the clinical CT exam. The study was approved by the local ethics review board and written informed consent was obtained.

CT imaging was performed using a third-generation dual-source CT (Siemens SOMATOM Force, Siemens Medical Solutions, Germany). A retrospective image acquisition with ECG-triggered dose modulation was used, resulting in images with 0.36x0.36x0.25 mm resolution and 20 time-frames covering the whole cardiac cycle. Following clinical protocol, data was acquired during inspiration breath-hold.

The MRI examination was performed using a clinical 3 T Philips Ingenia scanner (Philips Healthcare, the Netherlands). The 4D Flow data was acquired during free-breathing using a gradient-echo pulse-sequence with interleaved three-directional flow-encoding and retrospective vector cardiogram controlled cardiac gating and respiratory navigator gating at end-expiration. The acquired spatial resolution was 2.9x2.9x2.9 mm and the acquired temporal resolution was 40 ms. For details on imaging parameters, see (Lantz et al., 2018, 2016).

The clinical CT demonstrated that the patient had a moderately dilated LV with an end-diastolic volume of 248 ml, stroke volume of 84 ml, and moderately depressed LV function with an ejection fraction of 34%. The patient did not have mitral regurgitation. Heart rate in CT and MRI acquisitions were 60 and 62 beats per minute, respectively.

2.2. Flow model

The heart geometry in this study was an anatomically detailed cardiac model, including 17 pulmonary vein branches, left atrium and appendage, left ventricle including papillary muscles and trabeculae, and ascending aorta. Based entirely on the acquired CT images, intracardiac flow fields were computed (Lantz et al., 2018), where blood flow was modelled as laminar flow. The endocardial wall motion was extracted from the CT images using non-rigid registration (Gupta et al., 2018), and was prescribed in flow solver (CFX 17.0, Ansys Inc, Canonsburg). The aortic valve was modelled as being either opened or closed. The native mitral valve was modeled as either open or closed but moved with the valve plane. The native valve geometry was based on segmentations of the CT data at end-diastole and end-systole. The mechanical mitral valve was modelled as a generic bileaflet mechanical valve using an immersed boundary method Fig. 1 shows geometry of the mechanical valve. The diameter of the mechanical mitral valve was similar to the annulus of the native valve and the movement of the native annulus was imposed on the mechanical valve. The rotation of the leaflets was kinematically constrained between the closed (θ_{min} = 22°) and open (θ_{max} = 80°) positions, as indicated in Fig. 1B. The mechanical valve was oriented in 4 different positions, starting at the anatomical commissure-commissure position (corresponding to 0°) and rotated in-plane to 45°, 90° (anti-anatomical position) and 135°, see Fig. 1C. More details can be found in the appendix).

The temporal resolution of the simulations was 500 μs, and approximately 14 million computational cells were used, with the smallest length scale on the order of 50 μm to resolve high curvature regions. A 3-element Windkessel model was applied to the ascending aorta, which was tuned to match brachial blood pressure cuff measurements. The pulmonary venous artery tree con-

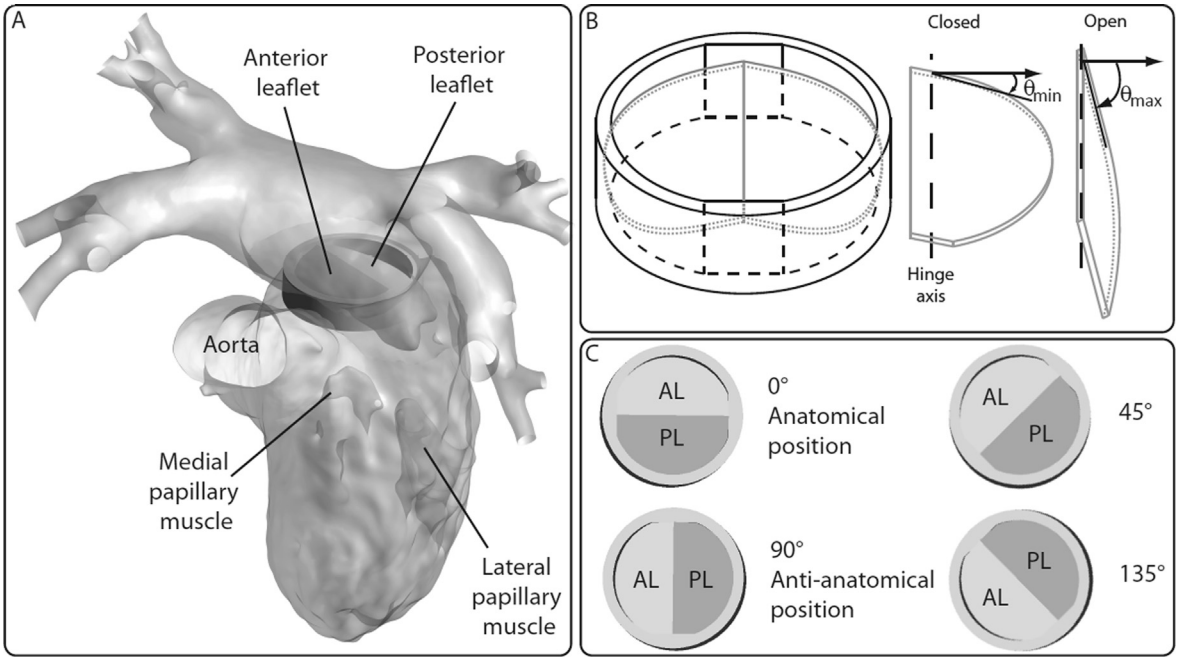

Fig. 1. The model used in the simulation. Panel A shows the positioning of the mechanical valve in the anatomical orientation (0°). Panel B depicts the prosthetic valve with leaflets in the closed and open positions (angles θ_{min} and θ_{max}, respectively). Panel C show the four valve orientations investigated in this study and how the axes of the anterior and posterior leaflets (AL and PL, respectively) are rotated.

sisted of 17 separate vessels that converged into four major veins that drained into the left atrium. At each of the 17 pulmonary vein inlets, a constant pressure of 10 mmHg was applied, as a first order approximation of the pulmonary capillary pressure (Casas et al., 2017; Lantz et al., 2019).

2.3. Evaluation

Intracardiac flow fields with a native mitral valve in place were measured with *in vivo* MRI and CT-based CFD and compared qualitatively as well as quantitatively. LV flow fields with a virtual bileaflet mechanical mitral valve were generated with CFD; fields calculated for 4 different valve orientations were compared.

Quantitative assessment of the prosthetic valve leaflets included timing and opening angle. The integrated diastolic kinetic energy was measured in the volumes of the LV basal, mid and apical zones to reflect the flow kinetics in these regions. Flow component analysis, which is commonly employed in cardiac 4D flow MRI (Bolger et al., 2007; Carlhäll and Bolger, 2010; Eriksson et al., 2010), was performed to quantify the effect of the mitral valve on the LV flow patterns. This type of flow analysis has been used in both healthy subjects and patients, and comparison has been performed between 4D flow MRI data and CT-based CFD simulations (Lantz et al., 2018) with good agreement. In short, cardiac flow patterns can be divided into four components:

- direct flow: enters the LV and leaves through the aorta in one heartbeat
- retained inflow: enters the LV and stays there for at least one heartbeat
- delayed ejection flow: currently in the LV and leaves into the aorta in the current heartbeat
- residual volume: currently in the LV and will stay there for at least one more heartbeat

Furthermore, the power loss during ventricular filling was computed. As energy is lost to heat due to high shear gradients by means of viscous dissipation, the amount of power loss for each valve orientation could potentially be an indicator of optimal placement. Power loss was computed as

$$\text{Power loss} = \int_V 2\mu S_{ij} \cdot S_{ij} dV \quad (1)$$

where μ is fluid viscosity and S_{ij} rate-of-deformation, with the volume integral taken over the LA, LV and mitral valve. While this calculation was feasible for CFD results, the low spatial resolution in 4D Flow MRI data significantly limits the accuracy for this type of calculation.

3. Results

3.1. Native mitral valve

Long axis planes through the LV and part of the left atrium in a standard 3-chamber orientation are shown in Fig. 2.

Velocities from MRI and CFD are shown with short streamlines to emphasize the direction of flow. Both MRI and CFD images demonstrate how the native valve directed mitral inflow towards the lateral wall. CFD simulation of the native valve demonstrates vortical structures at the base. Vortex rotation is shown using out-of-plane vorticity calculated from the long axis plane. During early diastolic filling, vortices formed on the ventricular surface of the anterior and posterior leaflets and in the planar cross section are seen to rotate clockwise (blue) and counterclockwise (red), respectively. The anterior part of the vortex, located in the central LV, is larger than the posterior part whose expansion is constrained by the adjacent inferolateral wall. Those vortices disperse during diastasis, and reform in a smaller size during the late filling phase.

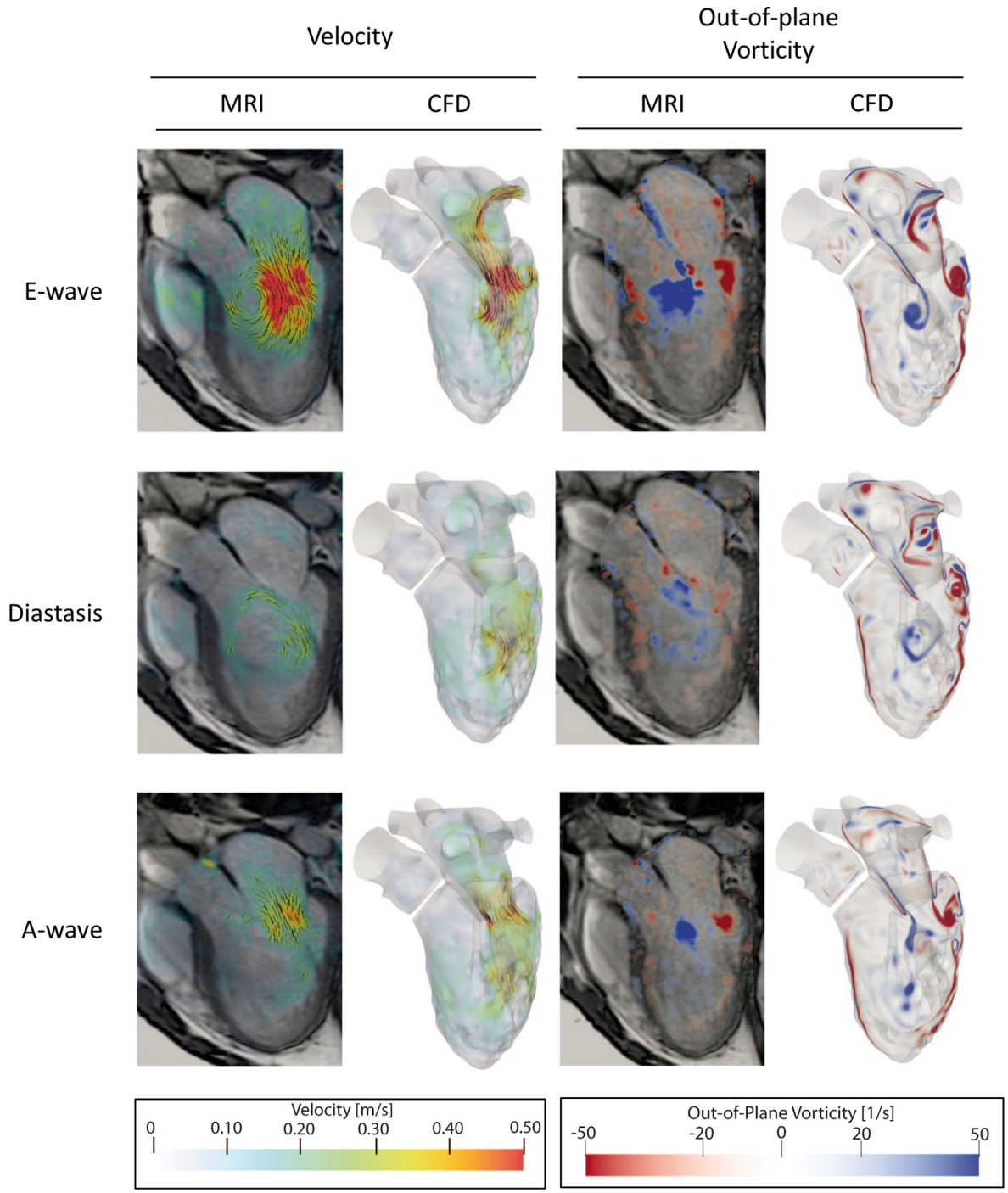

Fig. 2. In vivo MRI and CFD simulations of LV flow patterns for a native mitral valve. Velocity and out-of-plane vorticity are shown for early filling, diastasis and late filling phases.

3.2. Virtual mechanical mitral valve

3.2.1. LV flow patterns

LV flow patterns with the natural valve in short axis planes are shown in Fig. 2; LV flow patterns in the entire LV volume with the virtual mitral valve implanted with four different orientations are shown in Fig. 4. The mechanical mitral valve creates shear layers in the two leaflet orifices and the much smaller central orifice. The predominant flow was through the two leaflet orifices. The shear layers extend into the LV cavity and interact with each other. This interaction creates a complex vortex-rich flow pattern in the basal and mid regions of the ventricle.

The orientation of the mechanical valves determines the positions of the two dominant incoming flow jets at the base (Fig. 3). Highest flow velocities were closest to the leaflets and declined radially. Velocities also diminished from the base to the apex, indicating that most of the flow energy was located in the basal and mid regions. The double orifice inflow pattern seen in the basal plane breaks up into more complex structures in the mid and apical planes.

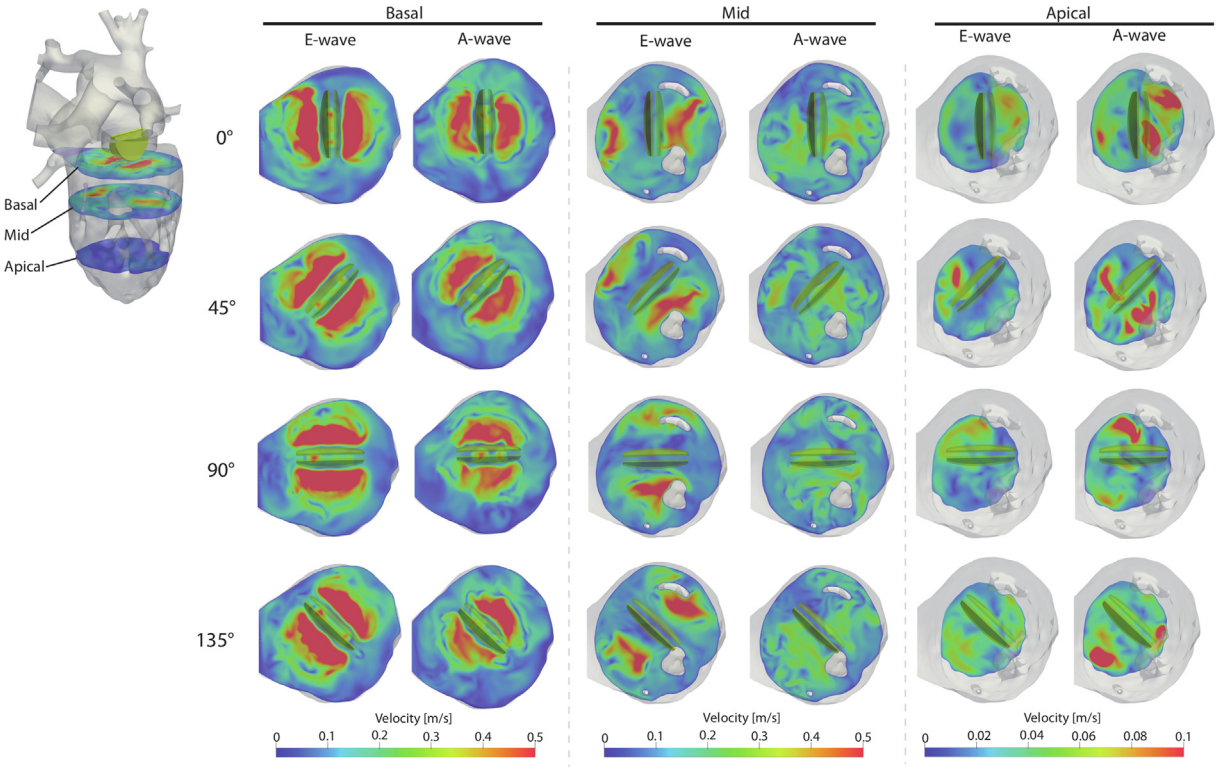

Fig. 3. Short axis flow patterns at basal, mid and apical LV levels showing velocity at early diastolic filling, diastasis and late diastolic filling. Mechanical valve leaflets are visualized in transparent yellow. Note the change in velocity scale for the apical velocities. (For interpretation of the references to colour in this figure legend, the reader is referred to the web version of this article.)

Early filling through the prosthetic valve flow was associated with vortex formation at the base; inflow was more centrally directed compared to native valve early flow. In all prosthetic orientations, high velocities and vortical flow were noted in the LV outflow tract, a region bounded by the anteroseptum and the aortic valve. With the native valve, this region was free from strong vortices or high diastolic velocities during all diastolic phases.

During diastasis the flow through the mitral valve was low. The large vortical structures seen during early filling dissipated into smaller vortices. Residual flow dynamics were present in the basal and mid regions; in the apical region, flow appeared relatively stationary with very low velocities and absence of vorticity.

During late diastolic filling when the left atrium contracts, a second vortex formed near the mitral valve leaflets. It was smaller compared to the early inflow vortex and was not limited to the inferolateral zone as seen with the native valve. With all valve orientations, the inflow jet did not penetrate as deeply into the LV cavity as with the native valve.

3.2.2. Flow component analysis

Flow component analysis of 4D MRI data has been used to demonstrate differences between healthy subjects and different patient groups (Bolger et al., 2007; Carlhäll and Bolger, 2010; Eriksson et al., 2010). In this study, flow components in the presence of a native valve were measured with both MRI and CFD (Table 1). Compared to 4D MRI, proportions of direct flow were slightly lower and residual volume slightly higher using CFD; retained inflow and delayed ejection flow were similar for both methods.

The flow component distribution after virtual mechanical valve implantation is also shown in Table 1. With the mechanical valve in place, the residual volume increased irrespective of the prosthetic orientation. This was apparent in Fig. 4, where the mitral inflow did not penetrate as deep into the LV cavity after valve implantation. The increase in residual volume was at the expense of the retained and delayed flow components, which decreased from 25 to 26% to 16–18%. The direct flow component increased from 2% for the CFD of the native valve to 7–8%, possibly related to more of the incoming flow staying in the basal region.

3.2.3. Power loss

Power loss due to viscous dissipation during diastole was calculated from time steps when the mitral valve was open. Power loss values for the native valve are low as calculated from the simulation as well as the 4D flow MRI measurements (Fig. 5). After valve

Table 1
Results from flow component analysis. The analysis was performed for both the native valve (MRI and CFD) as well as CFD simulations for 4 different orientations of the mechanical valve.

	Native valve		Mechanical valve			
Flow component	MRI	CFD	0°	45°	90°	135°
Direct flow [%]	6	2	7	8	8	8
Retained inflow [%]	25	25	16	18	17	17
Delayed ejection flow [%]	26	25	17	17	18	17
Residual volume [%]	43	48	60	57	57	58

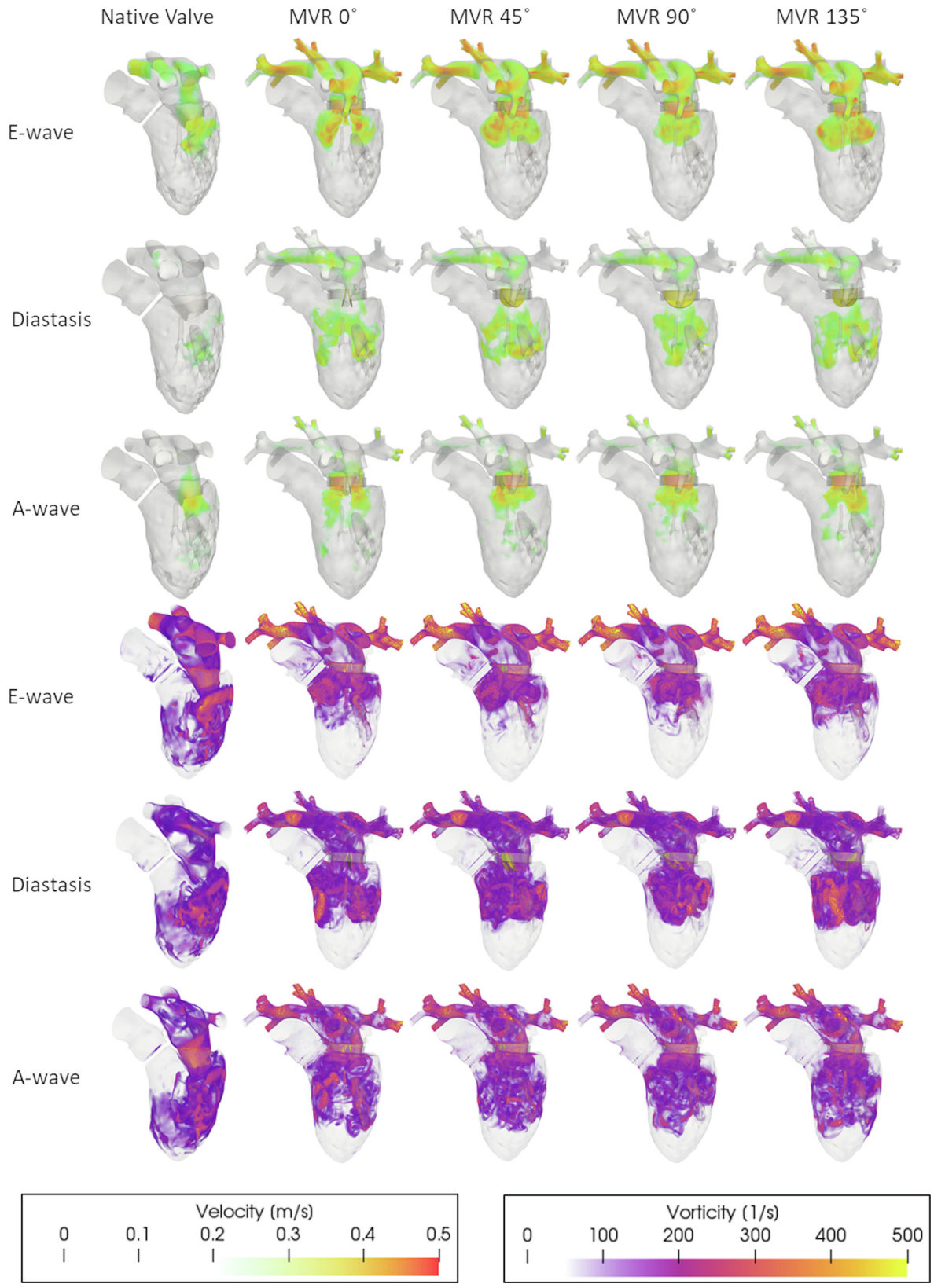

Fig. 4. CFD simulations of LV flow patterns with a native valve and with a virtual bileaflet mitral valve prosthesis oriented with 4 different angles. Flow velocity and vorticity are shown for early filling, diastasis and late filling phases.

implantation, the power loss increases with peak values approximately 3 times higher than the native valve. The higher values are a direct consequence of the high shear stresses in the mechanical valve, and are more pronounced during early filling when the flow is highest. Only minor differences in the four different mechanical valve orientations could be observed.

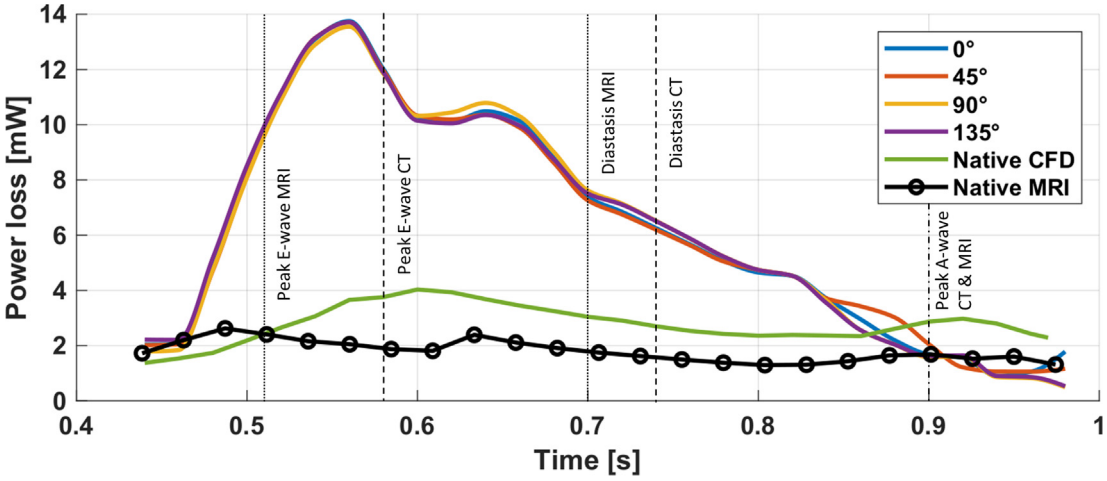

Fig. 5. Power loss due to viscous dissipation in the left heart during diastole. The four mechanical heart valve orientations all resulted in similar power losses, which were higher than losses for the native valve calculated from both CFD and 4D MRI data.

4. Discussion

In this study, we examined the impact of prosthetic valve implantation and the specific valve orientation on LV flow fields. To define the flow field prior to virtual mitral replacement, we utilized *in vivo* MRI and CT data to assess baseline conditions in a patient with a dilated, dysfunctional left ventricle and a competent native mitral valve. The baseline CFD simulation was used to assess the impact of valve replacement, and of different valve implantation orientations on LV flow patterns and parameters of efficiency and volume exchange. The patient's baseline abnormalities in LV size and function are common among patients undergoing mitral surgery. As assessed by flow component analysis using MRI data, the patient's baseline flow components were consistent with his pre-existing moderate heart failure. It is important to recognize that the patient's flow-based parameters were abnormal at baseline, and that any changes in those parameters would be incremental to those baseline abnormalities. A virtual mitral replacement in a patient with less abnormal flow at baseline might show different changes related to prosthetic orientation.

For the patient in this study, the native valve directed the mitral inflow towards the lateral wall and a large vortex was formed in the LV cavity during diastole. After implantation, the mechanical valve directed the inflow differently, towards the center of the LV. The ventricular flow became more complex with multiple vortical structures rather than the large central vortex identified with the native valve in place. The inflow did not penetrate into the LV cavity as deeply, so that more incoming flow stayed in the basal LV region. One consequence was that higher diastolic velocities and more vortical flow structures were present in the left ventricular outflow tract, which is not seen with the native valve.

With all valve orientations, the residual volume in the apical LV was seen to increase. Quantitatively, the flow component analysis confirmed the increase of the residual volume. This increase was in addition to the patient's baseline elevated residual volume, as compared to the range in normal subjects. Eriksson, et al., noted a range of LV residual volume of 35 ± 6% (mean ± SD) in patients with dilated cardiomyopathy (Eriksson et al., 2013). The patient in this study, with a residual volume of 48% at baseline, already had notable flow component distortion. Even so, following virtual mitral valve replacement the residual volume expanded to 57–60%, which may promote thrombus formation (Eriksson et al., 2010; Ziegler et al., 2019). Worsened apical stasis despite increased peak inflow velocities through a mitral prosthesis may appear counterintuitive to practitioners. Recognition that apical flow changes with MVR might contribute to the patient's postoperative thromboembolic risk, if proven, could refine the life-long anticoagulation strategies to which these patients are exposed.

Power loss due to viscous dissipation increased after valve implantation, which is a direct consequence of the higher shear stresses found in the mechanical valve. This indicates that the mechanical valve may be disadvantageous with respect to LV pumping efficiency (Bolger et al., 2007; Eriksson et al., 2010). The power losses of the four different valve orientations were similar, indicating that from that perspective there was no optimal placement for this patient.

This study represents one of the first cases where a mechanical mitral valve has been studied in an anatomically detailed cardiac geometry. It only represents one case, however, and differed in several ways from many patients undergoing mitral valve replacement or repair. The selected patient did not have mitral insufficiency, which would be significant in an actual valve recipient. The regurgitant jet of significant mitral insufficiency increases ventricular inflow and velocity in a manner that is not modelled in these simulations. The patient also had significant LV dysfunction and remodeling, and pre-implantation abnormalities of flow components that are quantitatively in range for other patients with moderate heart failure. Patients referred for mitral surgery present a wide spectrum of LV derangement, from worse than that seen in this patient to normal function. Larger prospective studies are required to establish the prognostic performance of valve implantation *in silico*. It is possible that patients with normal cardiac function or different ventricular geometry would be more affected by the specific orientation of the valve. The valve design modelled here was a generic bileaflet valve; other mechanical heart valves with different designs may result in more favorable flow patterns, which should be a topic for future studies. A strength of this framework is that it allows any type of mechanical valve to be assessed. Blood flow was modelled as laminar. Previously, we investigated turbulence in the left ventricle in patients with dilated cardiomyopathy using 4D flow MRI (Zajac et al., 2015). We found that in patients with larger left ventricles, higher turbulence occurs at peak A-wave compared to healthy volunteers, but levels seem to be relatively low. Further research is needed to determine, whether these levels of turbulence can be covered with the laminar flow model, or if a turbulence model provides more accurate results.

The wall-motion was extracted from CT data with a native valve and prescribed in the CFD solver for the simulation of the native

valve as well as the mechanical valves. Only the cardiac function at the time of CT acquisition was considered. Thus, any eventual changes in the geometry and function in the heart due to surgery or remodeling after the valve implantation are not reflected in the model. However, as both *in vivo* 4D flow MRI measurements and numerical simulations of the native valve were performed, the effect of valve implantation was able to be isolated and studied preoperatively. The setup of the simulation model took about 4 h of manual work. Most time was spent implanting the mechanical valve to the LV geometry which can be improved using tailored CAD software that can handle complex triangulated surfaces. Before larger clinical studies can be performed, this issue should be addressed.

In closing, using our numerical framework we were able to assess intraventricular flow fields before and after virtual implantation of a bileaflet mechanical mitral valve. Qualitative and quantitative changes in diastolic left ventricular blood flow were demonstrated after virtual mechanical mitral valve implantation compared to the native valve. In this subject with significant pre-existing ventricular dilation and hypokinesis, valve orientation had some effects on the complexity of left ventricular flow patterns, but did not impact overall diastolic power losses or flow component proportions. These patient-specific results highlight the close hemodynamic coupling between the flow effects of the mechanical valve and the pre-implantation cardiac function and geometry. The approach used in this study may be used to improve design of prosthetic heart valves and surgical valve replacement procedures, and could potentially assist in clinical treatment planning of patients with mitral valve disease.

Acknowledgements

The authors acknowledge funding from the Knut and Alice Wallenberg Foundation through the project *Seeing Organ Function*, from the Swedish Heart Lung Foundation, Vinnova, the Swedish Research Council, and the County Council of Östergotland. The simulations were performed on resources provided by the Swedish National Infrastructure for Computing (SNIC) at National Supercomputer Centre (NSC).

Appendix A

Materials and methods

Flow model

For the flow simulations, the end diastolic endocardial geometry was segmented from CT data. The motion was tracked over time using a non-rigid registration algorithm (Gupta et al., 2018).

The end diastolic mesh was generated using ICEM 17.0 (Ansys Inc., Canonsburg, PA). During the simulation, the mesh was deformed according to the motion calculated by the registration. Due to the large deformation of the heart, the topology of the mesh was adjusted every 25 msec. The flow simulation was done in CFX 17.0 (Ansys Inc., Canonsburg, PA) with a temporal resolution of 500 μsec. Blood was modelled as an incompressible, Newtonian fluid with a density of 1060 kg/m^3 and a viscosity of 3.5 e-3 Pa s. The flow was assumed to be laminar.

To remove any effects of initial conditions, several heart beats were simulated and the fourth and third cardiac cycle were analyzed for the native and mechanical mitral valve, respectively. The simulations took about 7 h per cardiac cycle on 96 cores (Intel Xeon E5-2660).

Mechanical valve dynamics

The mechanical valve consisted of three parts: a solid ring that moved with the valve plane, and two semicircular leaflets connected to the solid ring and allowed to rotate around a hinge axis, as shown in Fig. 1. The flow through the valve can be separated into three regions: two lateral and one central orifice, resulting in a triple jet pattern where most of the flow emerges from the lateral orifices. The leaflets were modeled as immersed solids using the CFX immersed solids module and their rotation dynamics around the hinge axis were determined by conservation of angular momentum as:

$$T = I\ddot{\theta} \tag{1}$$

where T was the applied torque from the fluid on each valve leaflet, I the moment of inertia (here set to 8.75e-9 kg m^2 , based on the geometry in the CAD software) and $\ddot{\theta}$ the angular acceleration. The rotation axis of the leaflets was implemented using in-house FORTRAN code. When the atrial pressure was greater than the ventricular pressure, the net torque on the leaflets resulted in an opening motion, and blood was allowed to flow from the atrium to the ventricle. Conversely, when ventricular pressure was greater than atrial pressure (as in systole) the net torque on the leaflets produced a closing motion. Equation (1) was implemented into the flow solver as:

$$\dot{\theta}^t = \dot{\theta}^{t-1} + \Delta t \frac{T}{I} \tag{2}$$

where $\dot{\theta}^t$ and $\dot{\theta}^{t-1}$ are the angular velocity at the current and previous time step, respectively, and Δt is the time step size. Additionally, the rotation was kinematically constrained between the closed (θ_{min} = 22°) and open (θ_{max} = 80°) positions, as indicated in Fig. 1B. When the leaflet was within 1 degree of being either fully opened or closed, an artificial damping torque was gradually added to make the leaflet come to a complete stop. The mechanical valve was oriented in 4 different positions, starting at the anatomical commissure-commissure position (corresponding to 0°) and rotated in-plane to 45°, 90° (anti-anatomical position) and 135°, see Fig. 1C.

Flow phases

To compare the different flow fields, we focused on three characteristic flow phenomena: peak E-wave, Diastasis, and peak A-wave. Peak E-wave and A-wave are characterized as the two maxima in the mitral valve flow and Diastasis is the minimum flow between the two maxima. The timing of these flow phenomena are shown in Table 2. Timing of diastole and systole is defined by the opening of the valves. The opening of the mitral valve differs slightly between the simulation of native valve and the simulation of the mechanical valve. In the simulation of the native valve, the opening of the mitral valve is defined by the motion of the ventricle. At the time when the ventricle is the smallest, the valve is forced to be open. In the simulation of the mechanical valve, however, the opening of the valve is driven by the pressure difference between ventricle and atrium. When the pressure in the atrium is

Table 2
Timing of the different phases of the cardiac cycle.

	MRI	Native valve	Mechanical Valve
Length of systole (s)	0.35	0.35	0.4
Peak E wave (s)	0.51	0.58	0.58
Diastasis (s)	0.7	0.74	0.74
Peak of A wave (s)	0.9	0.9	0.9
Length of Diastole (s)	0.62	0.65	0.6
Length of Cardiac Cycle (s)	0.97	1	1

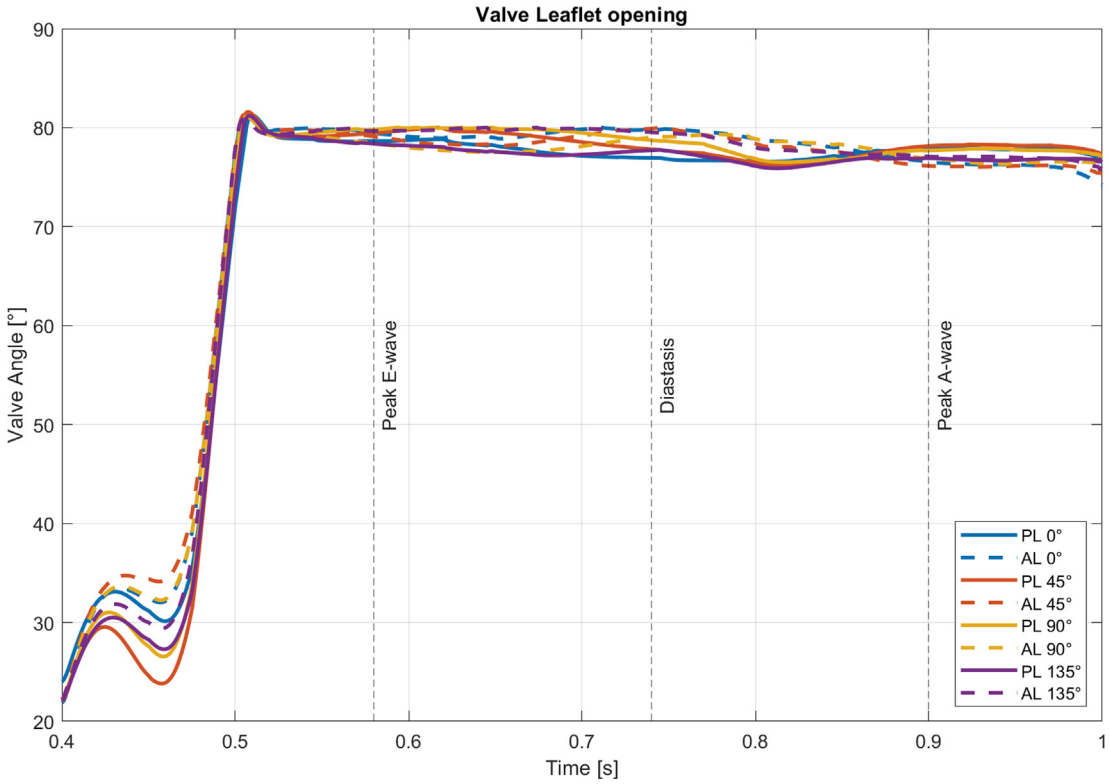

Fig. A1. Valve leaflet dynamics during diastole. Atrial contraction initiates the late filling phase at 0.9 s. PL and AL refer to the posterior and anterior leaflets, as defined in Fig. 1C.

higher than in the atrium, the valve opens. Therefore, the mechanical heart valve opens slightly later than the native valve.

Results

Mechanical valve leaflet dynamics

The leaflet opening dynamics for both the anterior (AL) and posterior (PL) leaflets were monitored for each time step to study potential asymmetry in the leaflet dynamics. As the leaflet rotation dynamics were a direct consequence of the net torque acting on each leaflet, local hemodynamics could potentially affect the leaflets differently. As seen in Fig. A1, there were slight differences in the leaflet dynamics. The initial opening motion of the leaflets from 0.40 to 0.46 s was driven by a slight excursion of the mitral annulus towards the atrium which lead to the anterior leaflet always opening faster than the posterior leaflet. The differences between the leaflets was greatest in the 45° orientation, and smallest in the 0° and 135° orientations. The rapid opening phase between 0.46 and 0.50 s was due to reversal of the atrioventricular pressure gradient, leading to the early diastolic filling phase. During this phase the leaflets of all the virtual valves opened with the same angular velocity until they reached the fully opened position. The leaflets stayed almost fully open during the second half of diastole (0.5 to 1 s), with only a minor drift from the fully open position ($\theta_{max} = 80°$) to approximately $\theta = 75°$ at the end of diastole. Of note, the atrial contraction in late diastole at 0.90 s did not force the leaflets to fully open.

Appendix B. Supplementary data

Supplementary data to this article can be found online at https://doi.org/10.1016/j.jbiomech.2020.110209.

References

Bianchi, M., Marom, G., Ghosh, R.P., Rotman, O.M., Parikh, P., Gruberg, L., Bluestein, D., 2019. Patient-specific simulation of transcatheter aortic valve replacement: impact of deployment options on paravalvular leakage. Biomech. Model. Mechanobiol. 18, 435–451. https://doi.org/10.1007/s10237-018-1094-8.

Bolger, A., Heiberg, E., Karlsson, M., Wigström, L., Engvall, J., Sigfridsson, A., Ebbers, T., Kvitting, J.-P.E., Carlhäll, C.J., Wranne, B., 2007. Transit of Blood Flow Through the Human Left Ventricle Mapped by Cardiovascular Magnetic Resonance. J. Cardiovasc. Magn. Reson. 9, 741–747. https://doi.org/10.1080/10976640701544530.

Cannegieter, S.C., Rosendaal, F.R., Briët, E., 1994. Thromboembolic and bleeding complications in patients with mechanical heart valve prostheses. Circulation 89, 635–641. https://doi.org/10.1161/01.CIR.89.2.635.

Carlhäll, C.J., Bolger, A., 2010. Passing strange: flow in the failing ventricle. Circ. Heart Fail. 3, 326–331. https://doi.org/10.1161/CIRCHEARTFAILURE.109.911867.

Casas, B., Lantz, J., Viola, F., Cedersund, G., Bolger, A.F., Carlhäll, C.-J., Karlsson, M., Ebbers, T., 2017. Bridging the gap between measurements and modelling: a cardiovascular functional avatar. Sci. Rep. 7, 6214. https://doi.org/10.1038/s41598-017-06339-0.

Chandran, K.B., 2010. Role of Computational Simulations in Heart Valve Dynamics and Design of Valvular Prostheses. Cardiovasc. Eng. Technol. 1, 18–38. https://doi.org/10.1007/s13239-010-0002-x.

Choi, Y.J., Vedula, V., Mittal, R., 2014. Computational study of the dynamics of a bileaflet mechanical heart valve in the mitral position. Ann. Biomed. Eng. 42, 1668–1680. https://doi.org/10.1007/s10439-014-1018-4.

Dyverfeldt, P., Bissell, M., Barker, A.J., Bolger, A.F., Carlhäll, C.J., Ebbers, T., Francios, C. J., Frydrychowicz, A., Geiger, J., Giese, D., Hope, M.D., Kilner, P.J., Kozerke, S., Myerson, S., Neubauer, S., Wieben, O., Markl, M., 2015. 4D flow cardiovascular magnetic resonance consensus statement. J. Cardiovasc. Magn. Reson. 17, 72. https://doi.org/10.1186/s12968-015-0174-5.

Eriksson, J., Bolger, A.F., Ebbers, T., Carlhäll, C.J., 2013. Four-dimensional blood flow-specific markers of LV dysfunction in dilated cardiomyopathy. Eur. Heart J. Cardiovasc. Imaging 14, 417–424. https://doi.org/10.1093/ehjci/jes159.

Eriksson, J., Carlhäll, C.J., Dyverfeldt, P., Engvall, J., Bolger, A.F., Ebbers, T., 2010. Semi-automatic quantification of 4D left ventricular blood flow. J. Cardiovasc. Magn. Reson. 12, 9. https://doi.org/10.1186/1532-429X-12-9.

Faludi, R., Szulik, M., D'hooge, J., Herijgers, P., Rademakers, F., Pedrizzetti, G., Voigt, J.-U., 2010. Left ventricular flow patterns in healthy subjects and patients with prosthetic mitral valves: An in vivo study using echocardiographic particle image velocimetry. J. Thorac. Cardiovasc. Surg. 139, 1501–1510. https://doi.org/10.1016/J.JTCVS.2009.07.060.

Garitey, V., Gandelheid, T., Fuseri, J., Pélissier, R., Rieu, R., 1995. Ventricular flow Dynamic past Bileaflet Prosthetic Heart Valves. Int. J. Artif. Organs 18, 380–391. https://doi.org/10.1177/039139889501800706.

Gupta, V., Lantz, J., Henriksson, L., Engvall, J., Karlsson, M., Persson, A., Ebbers, T., 2018. Automated three-dimensional tracking of the left ventricular myocardium in time-resolved and dose-modulated cardiac CT images using deformable image registration. J. Cardiovasc. Comput. Tomogr. 12, 139–148. https://doi.org/10.1016/j.jcct.2018.01.005.

Lantz, J., Gupta, V., Henriksson, L., Karlsson, M., Persson, A., Carlhäll, C.-J., Ebbers, T., 2019. Impact of Pulmonary Venous Inflow on Cardiac Flow Simulations: Comparison with In Vivo 4D Flow MRI. Ann. Biomed. Eng. 47, 413–424. https://doi.org/10.1007/s10439-018-02153-5.

Lantz, J., Gupta, V., Henriksson, L., Karlsson, M., Persson, A., Carlhäll, C.-J., Ebbers, T., 2018. Intracardiac Flow at 4D CT: Comparison with 4D Flow MRI. Radiology 289, 51–58. https://doi.org/10.1148/radiol.2018173017.

Lantz, J., Henriksson, L., Persson, A., Karlsson, M., Ebbers, T., 2016. Patient-Specific Simulation of Cardiac Blood Flow From High-Resolution Computed Tomography. J. Biomech. Eng. 138. https://doi.org/10.1115/1.4034652.

Laplace, G., Lafitte, S., Labèque, J.-N., Perron, J.-M., Baudet, E., Deville, C., Roques, X., Roudaut, R., 2004. Clinical significance of early thrombosis after prosthetic mitral valve replacement. J. Am. Coll. Cardiol. 43, 1283–1290. https://doi.org/10.1016/j.jacc.2003.09.064.

Laub, G.W., Muralidharan, S., Pollock, S.B., Adkins, M.S., McGrath, L.B., 1992. The experimental relationship between leaflet clearance and orientation of the St. Jude Medical valve in the mitral position. J. Thorac. Cardiovasc. Surg. 103, 638–641.

Mächler, H., Perthel, M., Reiter, G., Reiter, U., Zink, M., Bergmann, P., Waltensdorfer, A., Laas, J., 2004. Influence of bileaflet prosthetic mitral valve orientation on left ventricular flow - An experimental in vivo magnetic resonance imaging study. European Journal of Cardio-Thoracic Surgery. Narnia, 747–753. https://doi.org/10.1016/j.ejcts.2004.06.019.

Mächler, H., Reiter, G., Perthel, M., Reiter, U., Bergmann, P., Zink, M., Rienmüller, R., Laas, J., 2007. Influence of a tilting prosthetic mitral valve orientation on the left ventricular flow — an experimental in vivo magnetic resonance imaging study. Eur. J. Cardio-Thoracic Surg. 32, 102–107. https://doi.org/10.1016/j.ejcts.2007.02.038.

Meschini, V., de Tullio, M.D., Querzoli, G., Verzicco, R., 2018. Flow structure in healthy and pathological left ventricles with natural and prosthetic mitral valves. J. Fluid Mech. 834, 271–307. https://doi.org/10.1017/jfm.2017.725.

Nguyen, Y.N., Ismail, M., Kabinejadian, F., Tay, E.L.W., Leo, H.L., 2018. Post-operative ventricular flow dynamics following atrioventricular valve surgical and device therapies: A review. Med. Eng. Phys. 54, 1–13. https://doi.org/10.1016/j.medengphy.2018.01.007.

Pibarot, P., Dumesnil, J.G., 2009. Prosthetic heart valves: Selection of the optimal prosthesis and long-term management. Circulation. https://doi.org/10.1161/CIRCULATIONAHA.108.778886.

Pierrakos, O., Vlachos, P.P., 2006. The effect of vortex formation on left ventricular filling and mitral valve efficiency. J. Biomech. Eng. 128, 527–539. https://doi.org/10.1115/1.2205863.

Pierrakos, O., Vlachos, P.P., Telionis, D.P., 2004. Time-resolved DPIV analysis of vortex dynamics in a left ventricular model through bileaflet mechanical and porcine heart valve prostheses. J. Biomech. Eng. 126, 714–726. https://doi.org/10.1115/1.1824124.

Querzoli, G., Fortini, S., Cenedese, A., 2010. Effect of the prosthetic mitral valve on vortex dynamics and turbulence of the left ventricular flow. Phys. Fluids 22, 1–10. https://doi.org/10.1063/1.3371720.

Saaid, H., Segers, P., Novara, M., Claessens, T., Verdonck, P., 2018. Single calibration multiplane stereo-PIV: the effect of mitral valve orientation on three-dimensional flow in a left ventricle model. Exp. Fluids 59, 49. https://doi.org/10.1007/s00348-018-2504-5.

Singh-Gryzbon, S., Ncho, B., Sadri, V., Bhat, S.S., Kollapaneni, S.S., Balakumar, D., Wei, Z.A., Ruile, P., Neumann, F.J., Blanke, P., Yoganathan, A.P., 2020. Influence of Patient-Specific Characteristics on Transcatheter Heart Valve Neo-Sinus Flow: An In Silico Study. Ann. Biomed. Eng. 1–12. https://doi.org/10.1007/s10439-020-02532-x.

Sotiropoulos, F., Le, T.B., Gilmanov, A., 2016. Fluid Mechanics of Heart Valves and Their Replacements. Annu. Rev. Fluid Mech. 48, 259–283. https://doi.org/10.1146/annurev-fluid-122414-034314.

Stijnen, J.M.A., Van De Vosse, F.N., Baaijens, F.P.T., 2001. Influence of prosthetic mitral valve orientation on left ventricular flow, in. Computers in Cardiology. IEEE, 173–175. https://doi.org/10.1109/CIC.2001.977619.

Van Rijk-Zwikker, G.L., Delemarre, B.J., Huysmans, H.A., 1996. The orientation of the bi-leaflet CarboMedics valve in the mitral position determines left ventricular spatial flow patterns. Eur. J. Cardio-thoracic Surg. 10, 513–520. https://doi.org/10.1016/S1010-7940(96)80417-9.

Walczak, L., Georgii, J., Tautz, L., Neugebauer, M., Wamala, I., Sündermann, S., Falk, V., Hennemuth, A., 2019. Using Position-Based Dynamics for Simulating the Mitral Valve in a Decision Support System. Vis. Comput. Biol. Med, Eurographics Work.

Westerdale, J.C., Adrian, R., Squires, K., Chaliki, H., Belohlavek, M., 2015. Effects of Bileaflet Mechanical Mitral Valve Rotational Orientation on Left Ventricular Flow Conditions. Open Cardiovasc. Med. J. 9, 62–68. https://doi.org/10.2174/1874192401509010062.

Wu, W., Pott, D., Mazza, B., Sironi, T., Dordoni, E., Chiastra, C., Petrini, L., Pennati, G., Dubini, G., Steinseifer, U., Sonntag, S., Kuetting, M., Magliavacca, F., 2016. Fluid – Structure Interaction Model of a Percutaneous Aortic Valve : Comparison with an In Vitro Test and Feasibility Study in a Patient- Specific Case. Ann. Biomed. Eng. 44, 590–603. https://doi.org/10.1007/s10439-015-1429-x.

Yoganathan, A.P., He, Z., Casey Jones, S., 2004. Fluid Mechanics of Heart Valves. Annu. Rev. Biomed. Eng. 6, 331–362. https://doi.org/10.1146/annurev.bioeng.6.040803.140111.

Zajac, J., Eriksson, J., Dyverfeldt, P., Bolger, A.F., Ebbers, T., Carlhäll, C.-J., 2015. Turbulent kinetic energy in normal and myopathic left ventricles. J. Magn. Reson. Imaging 41, 1021–1029. https://doi.org/10.1002/jmri.24633.

Ziegler, M., Welander, M., Lantz, J., Lindenberger, M., Bjarnegård, N., Karlsson, M., Ebbers, T., Länne, T., Dyverfeldt, P., 2019. Visualizing and quantifying flow stasis in abdominal aortic aneurysms in men using 4D flow MRI. Magn. Reson. Imaging 57, 103–110. https://doi.org/10.1016/j.mri.2018.11.003.